Coverage-Dependent Infrared Spectroscopy of Carbon Monoxide on Iridium(111) in Aqueous Solution: A Benchmark Comparison between Chemisorption in Ordered Electrochemical and Ultrahigh-Vacuum Environments

Catherine Tang,[†,‡] Shouzhong Zou,[†] Mark W. Severson,[§] and Michael J. Weaver*[,†]

Department of Chemistry, Purdue University, West Lafayette, Indiana 47907; Department of Chemistry, National Tsinghua University, Hsinchu 30043, Taiwan; and Department of Chemistry, Oakland University, Rochester, Michigan 48309

Received: May 7, 1998; In Final Form: August 17, 1998

In-situ infrared reflection−absorption spectra (IRAS) measured for the C−O stretch (ν_{CO}) of carbon monoxide on ordered Ir(111) in aqueous 0.1 M $HClO_4$ as a function of the dosed coverage, θ_{CO}, are compared with corresponding extant IRAS data on Ir(111) in ultrahigh vacuum (UHV) in order to elucidate the physical influences exerted by the electrochemical double layer on chemisorbate vibrational properties. Unlike most metal surfaces, CO chemisorption on Ir(111) exhibits a lone ν_{CO} band consistent with a single (atop) binding site in both electrochemical and UHV environments over the entire coverage range up to saturation and features sizable θ_{CO}-dependent changes in the ν_{CO} frequency and other spectral parameters, reflecting adsorbate−adsorbate interactions. This surface−chemisorbate system therefore provides an unusual opportunity to explore in detail solvation and related environmental factors at the same stable (unreconstructed) metal substrate in the absence of additional "chemical" effects associated with coverage- and/or solvent-induced alterations in CO binding geometry. The nature of the vibrational interactions is assessed in part by comparing the θ_{CO}-dependent spectral parameters with predictions from a numerical dipole-coupling analysis. The electrochemical ν_{CO} peak frequencies, ν_{CO}^{p}, exhibit a marked dependence upon θ_{CO} that is comparable to that observed for the Ir(111)−UHV system. Similar saturation coverages, $\theta_{CO} \approx 0.7$, are also attained. Furthermore, the θ_{CO}-dependent ν_{CO}^{p} values are approximately coincident once the differences in surface work function in these two environments are taken into account by means of a Stark-tuning analysis. However, the integrated ν_{CO} band absorbance A_i displays a notably different dependence on θ_{CO} at the electrochemical and UHV-based interfaces, the former plot having a markedly less nonlinear shape than the latter. These differences can be understood in terms of solvent dielectric-screening effects, which attenuate the former A_i values at low θ_{CO}. The bandwidths, $\Delta\nu_{1/2}$, at the electrochemical interface are markedly (2−3-fold) larger at low and moderate θ_{CO} values compared to the UHV case. The former $\Delta\nu_{1/2}-\theta_{CO}$ behavior is indicative of stochastic broadening associated with microscopic variations in oscillator density incurred by random chemisorption. The Lorentzian ν_{CO} band shapes (for $\theta_{CO} > 0.4$) suggest that solvation-induced inhomogeneous line broadening is less important. The smaller $\Delta\nu_{1/2}$ values and curvilinear $\Delta\nu_{1/2}-\theta_{CO}$ behavior observed for the UHV system are consistent with local chemisorbate island formation. Nevertheless, for coverages approaching saturation ($\theta_{CO} \approx 0.7$) the electrochemical $\Delta\nu_{1/2}$ values diminish to a value, 7 cm^{-1}, only slightly broader than that (5 cm^{-1}) observed for the solvent-free UHV system. The A_i value attained at saturation for the electrochemical interface approaches that observed for the UHV system, the remaining dissimilarity being roughly consistent with the likely differences in the IRAS optical geometry.

Introduction

As is now well documented,[1,2] recent years have witnessed rapid (and ongoing) advances in our microscopic-level physical understanding of structure and bonding at electrochemical interfaces. This has been driven in part by the emergence of a swath of spectroscopic and spatial microscopic techniques applicable to in-situ metal−solution interfaces, together with the development of reliable as well as straightforward means of preparing ordered single-crystal metal surfaces for electrochemical purposes.[1] As a result, "electrochemical surface science" has become a coherent and broad-based discipline with increasingly close (and multifaceted) ties to ultrahigh-vacuum (UHV) surface science. One of the central fundamental issues prompted by these developments is elucidating the manner and extent to which chemisorbate structure and bonding at metal surfaces may be altered by the combined presence of solvent and electronic/ionic charges in electrochemical systems. The advent of infrared reflection−absorption spectroscopy (IRAS) as a sensitive in-situ probe of adsorption at monocrystalline metal−solution interfaces over the past decade[3] has provided substantial insight along these lines, especially when linked to IRAS measurements for related metal−UHV systems.[3c,4,5] Carbon monoxide has proved to be the archetype chemisorbate

* Corresponding author. Tel (765) 494-5466, FAX (765) 494-0239, e-mail: weaver@chem.purdue.edu.
[†] Purdue University.
[‡] National Tsinghua University.
[§] Oakland University.

10.1021/jp982156f CCC: $15.00
Published on Web 10/07/1998

for this purpose, stemming from the sensitivity of the C−O stretching (ν_{CO}) vibrational properties to the binding geometry and the local chemical and electrostatic interfacial environment.[3−5] The widespread availability of corresponding IRAS (and other structural data) for CO adsorbed either alone, or with selected coadsorbates, on the same metal surfaces in UHV provides another rich dimension in data interpretation. As a consequence, examining the form of the ν_{CO} spectra as a function of CO coverage (θ_{CO}) and electrode potential at ordered metal−solution interfaces in comparison with θ_{CO}-dependent spectra on the same metals in UHV can yield detailed information on the additional physical factors that control the more ornate electrochemical systems.[4,5]

Studies along these lines in our laboratory have included undertaking both in-situ electrochemical IRAS measurements for CO (and for the related chemisorbate NO) on various low-index Pt-group metals in nonaqueous[6] as well as aqueous media[4,7−10] and UHV-based "electrochemical modeling" studies.[5,11,12] The latter entail sequential low-temperature dosing onto the clean ordered surface in UHV of the various components (chemisorbate, solvent, ionic/electronic charge) that together constitute the so-called electrochemical "double layer".[13,14] Examining the response of the chemisorbate (and solvent) vibrational spectra to progressive alterations in the UHV-based interfacial composition can yield considerable insight into the nature of the inherently coupled solvation/electrostatic charge effects wrought by the double layer on the chemisorbate properties.[5] These effects include solvent-induced alterations in the spatial chemisorbate structure,[10] especially binding geometries,[11b−e] and those attributable directly to the combined influence of solvated ionic charge and dipolar solvent on the electrostatic field experienced by the chemisorbate.[11,12] The latter influence, collectively constituting the so-called "Stark-tuning" effect, is commonly manifested for in-situ electrochemical systems as shifts in the chemisorbate vibrational frequency as a function of the electrode potential.[15,16] Indeed, near-identical ν_{CO} frequency−surface potential behavior has been observed for saturated CO adlayers on Pt(111) in both in-situ electrochemical and UHV-based environments in the presence of various solvents once the potential values are converted to a common reference scale (vide infra).[11a] The observed frequency shifts can contain dominant contributions from potential-dependent metal−chemisorbate charge sharing as well as directly from the effect of the interfacial electrostatic field itself on the C−O bond.[15]

For most low-index Pt-group metals, the observed aqueous double-layer effects on the ν_{CO} spectra indicate that a combination of CO binding-site and Stark-tuning shifts is occurring, as reflected in often-marked θ_{CO}-dependent spectral differences, particularly regarding the occupancy of atop and multifold sites in comparison with the charge-/solvent-free interface in UHV. Clear-cut examples include the simple hexagonal close-packed (111) planes of platinum,[4,17] rhodium,[4] and palladium,[8b] for which possible complications from surface reconstruction will be absent. Unusually simple behavior is obtained on iridium(111), however, the θ_{CO}-dependent spectra featuring only a *single* ν_{CO} band, which is also maintained throughout the accessible electrode-potential range.[7c] This spectral fingerprint is suggestive of atop (or near-atop) CO coordination, even though the ν_{CO} frequency blue-shifts considerably (by ca. 60 cm^{-1}) with increasing θ_{CO}.[7c] Furthermore, closely similar θ_{CO}-dependent ν_{CO} spectra have been reported recently on clean Ir(111) in UHV, which are noted to also be consistent with essentially single-site (atop) CO coordination.[18] Comparable θ_{CO}-dependent ν_{CO} behavior is apparently also observed on Ir(110) in the aqueous electrochemical[7b] and UHV environments,[19] although the surface atomic structure is complicated by reconstruction.

These behavioral similarities, especially on the structurally simple (and stable) Ir(111) surface, encouraged us to reexamine the θ_{CO}-dependent ν_{CO} spectral properties on Ir(111) in acidic aqueous media, in part so to facilitate a detailed comparison with corresponding results for the solvent/charge-free UHV-based system. The salient findings of this study, along with a brief comparative examination of the ν_{CO} spectra on Ir(110), are reported herein. Emphasis is placed on quantitative comparisons of the θ_{CO}-dependent ν_{CO} frequencies, integrated band intensities, and bandwidths between the aqueous electrochemical and UHV-based interfaces and with the predictions of dipole-coupling models. The results provide unusual insight into the detailed physical effects of the aqueous solvating environment on the infrared properties of chemisorbed CO in the absence of obfuscating "chemical" effects associated with double-layer-induced alterations in binding-site geometries. As such, the system appears to provide a benchmark comparison between molecular chemisorbate vibrational properties at in-situ electrochemical and solvent-free metal−UHV interfaces.

Experimental Section

Details of the in-situ IRAS instrumentation and procedures are largely as outlined in refs 17 and 20. The FTIR spectrometer was a Mattson RS-2 instrument, with a custom-built external reflection compartment containing the narrow-band MCT detector. The spectral resolution was 1−2 cm^{-1} (vide infra). The glass spectroelectrochemical cell contains a detachable beveled CaF_2 window, forming the base of the vertically oriented cell, which slots into an opening on top of the N_2-purged external optical compartment. This design (from Prof. Carol Korzeniewski) obviates the need for additional N_2 purging after aligning the cell. The disk electrode, mounted on a glass plunger by wrapping with Teflon tape, was pressed against the CaF_2 window so to form the desired spectroelectrochemical thin layer.

The Ir(111) and (110) crystals, ca. 1 cm diameter, were procured from the Material Preparation Facility at Cornell University. They were oriented at least within 1°, as verified by X-ray diffraction. They were repolished with diamond paste to 0.25 μm grain size and then flame-annealed at 1500−1700 °C in an oxy-gas flame for ca. 15 min, to the point where the voltammetric features in 0.1 M $HClO_4$ were unchanged and characteristic of the well-ordered surfaces.[21−23] The crystal was cooled prior to electrochemical or spectroelectrochemical inspection in a fast-flowing H_2/Ar stream, followed by immersion in ultrapure water. Clean transferral to the electrochemical cell was facilitated by retaining a drop of water upon emersion. Successive annealings during each run required heating to 1500−1700 °C for only ca. 5−10 s. [Note that the above surface pretreatment differs from that used in our earlier IRAS study of the Ir(111)/CO system, which entailed forming a protective iodine layer during post-anneal cooling.[7c] The present procedure appears to yield a higher quality ordered surface on the basis of voltammetric and IRAS data (vide infra).[21]] Carbon monoxide (Matheson Gases) was 99.99% minimum, packed in an aluminum cylinder (thus avoiding the iron carbonyl contaminants often present in gas stored in steel cylinders). Electrolytes were prepared from concentrated perchloric acid (double distilled, GFS Chemicals) using ultrapure water (Millipore MilliQ). The reference electrode was Ag/AgCl (Bioanalytical Systems), but all electrode potentials are quoted here

versus the standard hydrogen electrode (SHE). All measurements were made at room temperature, 23 ± 1 °C.

Results and Data Analysis

Following voltammetric characterization of the freshly reannealed Ir(111) crystal[21] and further transferral to the spectroelectrochemical cell (vide infra), the surface was immersed in the deaerated 0.1 M $HClO_4$ electrolyte at 0.3−0.4 V (vs SHE). The irreversibly adsorbed CO adlayer was then formed by briefly (1−3 s) bubbling in CO followed by argon sparging so to remove almost all the solution CO before forming the spectroelectrochemical thin layer. This procedure is similar to that followed earlier for dosing CO adlayers on other Pt-group surfaces [e.g., Pt(111)[17]], although the unusually strong chemisorption on Ir(111) obliged the use of especially dilute CO solutions and/or short surface exposure times. The ν_{CO} spectra for a given dosed adlayer was then obtained by acquiring typically 100 interferometer scans at the desired electrode potential followed by a "reference spectrum" measured immediately after stepping to 0.75 V so to completely electrooxidize the adsorbed CO to CO_2. As usual,[17,20] subtracting the latter from the former spectrum removed the bulk solvent and other unwanted spectral features, yielding a potential-difference infrared (PDIR) spectrum[20] consisting of the desired C−O stretching (ν_{CO}) band along with a sharp opposite-polarity feature at 2343 cm^{-1} due to the O−C−O asymmetric stretch of the CO_2 product trapped in the thin layer. The surface remained well ordered during the PDIR measurements, as evidenced from the essentially identical spectra obtained upon subsequent solution CO dosing. Voltammograms for the oxidation of CO adlayers typically yielded extremely sharp anodic peaks, especially at high coverages, centered at about 0.65 V. The "sharper" nature of these peaks compared with those from our earlier study[7c] provides further evidence of the more ordered state of the present Ir(111) surface.

As documented in detail elsewhere,[17,24] the peak intensity of the CO_2 infrared feature, A_p, can be used to provide a reliable (±5−10%) estimate of the CO surface concentration, Γ_{CO}, and hence the CO coverage, θ_{CO}. This procedure, however, requires a calibration factor to enable the extraction of absolute adsorbate coverages from the measured A_p values. Given that the calibration is significantly dependent upon the precise spectrometer optical arrangement (vide infra), this is most reliably achieved by evaluating A_p for a given saturated CO adlayer having a known (and readily reproducible) Γ_{CO} (or θ_{CO}) value.[24] Fortunately, a recently described coulometric procedure has yielded accurate absolute coverages for saturated irreversibly adsorbed CO adlayers on a number of low-index Pt-group electrodes.[25] Comparing the CO_2 A_p values obtained from the oxidation of several saturated CO adlayers, including those on Ir(111), Ir(110), and Pt(111), with the corresponding coulometric Γ_{CO} values evaluated at potentials in the so-called "double-layer" potential region, 0.25−0.5 V, below the onset of CO electrooxidation, yielded consistently concordant results (relative Γ_{CO} values within ca. 5−10%). [Note that small apparent disparities in effective Γ_{CO} values between the coulometric and spectrophotometric values (say, ∼5%) can arise from procedural variations, leakage of CO_2 from the spectral thin layer, or slight differences in surface state.] This analysis yielded a saturated θ_{CO} value, θ_{CO}^{sat} [i.e., the Γ_{CO} value normalized to the Ir(111) surface atomic density, 1.57×10^{15} atoms cm^{-2}], equal to 0.60 ± 0.03 over the potential region 0.25−0.45 V. Interestingly, a significantly higher θ_{CO}^{sat} value, 0.72 ± 0.03, was obtained from spectrophotometry for irreversibly adsorbed CO dosed at −0.05 to 0.1 V, i.e., within the so-called "hydrogen region" where atomic hydrogen rather than water will be the predominant coadsorbate. A qualitatively similar, yet more pronounced, potential-induced variation in θ_{CO}^{sat} was observed in the earlier study of Ir(111)/CO from this laboratory, albeit with a less well-ordered substrate (vide supra).[7c] This point is returned to below.

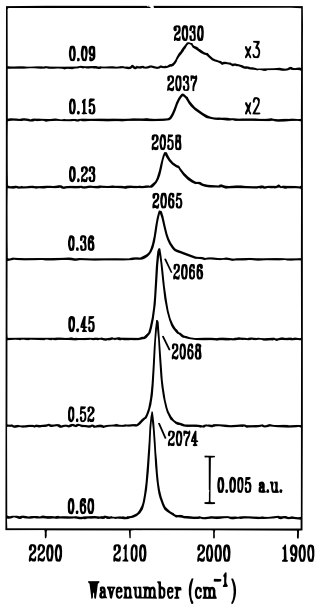

Figure 1. Infrared absorbance spectra (intensities in $\log_{10}$ absorbance units, au) for dosed CO coverages, as indicated, on ordered Ir(111) at 0.4 V vs SHE in aqueous 0.1 M $HClO_4$.

This procedure therefore enabled ν_{CO} spectra to be obtained for dosed CO adlayers over a wide range of reliably known θ_{CO} values, from 0.05 up to saturation. A typical set of θ_{CO}-dependent ν_{CO} spectra (intensity scale in $\log_{10}$ absorbance units, au) obtained at 0.4 V is shown in Figure 1; the θ_{CO} values are indicated beside each spectrum. A notable feature is the presence of a single ν_{CO} band throughout the observed θ_{CO} range, which both sharpens and blue-shifts substantially (by ca. 45 cm^{-1}) as the coverage increases up to saturation. As considered further below, these spectral fingerprints are closely reminiscent of the observed θ_{CO}-dependent behavior of the Ir(111)−UHV system.[18] Roughly comparable θ_{CO}-dependent ν_{CO} spectra to Figure 1 were obtained in the earlier study, although the bands were generally broader,[7c] again suggestive of a less well-ordered Ir(111) surface than that attained here.

While we are concerned here chiefly with CO chemisorption within the double-layer potential region where water coadsorption is involved, the significantly higher saturation coverage attainable by CO dosing at low potentials also gives rise to interesting ν_{CO} spectra. A comparison between a pair of ν_{CO} spectra both obtained for saturated irreversibly adsorbed adlayers at 0.4 V, but formed by CO dosing at 0.4 V and at a lower potential, 0.05 V (i.e., within the hydrogen region), before adjustment to 0.4 V is shown in Figure 2A and B, respectively. (An essentially identical ν_{CO} spectrum to (B) is also obtained by CO dosing *and* measurement at 0.05 V, except that the band frequency is slightly, 8 cm^{-1}, red-shifted compared to the value at 0.4 V, as expected from the Stark-tuning effect.[7c]) The θ_{CO}^{sat} value corresponding to the spectrum in (B) (as obtained from the CO_2 band intensity), 0.72, is decidedly higher than for the spectrum in (A), 0.60. This 20% difference in θ_{CO}^{sat} is also reflected in a 25% difference in the integrated absorbance, A_i, of the ν_{CO} band. Spectra were also obtained as in Figure 2A and B, but in the presence of near-saturated (ca. 1 mM) CO-

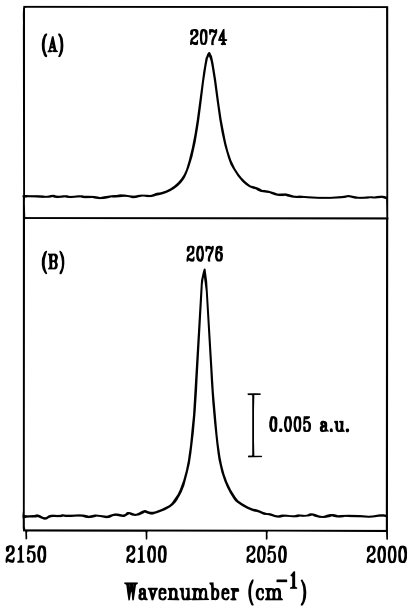

Figure 2. Infrared absorbance spectra for saturated irreversibly adsorbed CO adlayers on ordered Ir(111) at 0.4 V in 0.1 M $HClO_4$. Spectra in (A) and (B) formed by CO dosing at 0.4 and 0.05 V, respectively (see text).

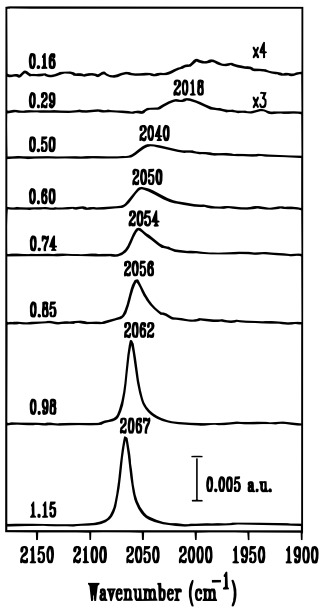

Figure 3. As for Figure 1, but for CO coverages, as indicated, on ordered Ir(110) at 0.35 V vs SHE.

containing electrolyte (i.e., without Ar solution sparging prior to data acquisition). This modification yielded virtually no effect on the spectrum obtained after lower-potential dosing (Figure 2B), suggesting further that this condition refers to "true" adlayer saturation. However, the presence of solution CO altered significantly the peak frequency, absorbance, and bandwidth of the ν_{CO} feature obtained by dosing at 0.4 V, yielding a spectrum intermediate between those observed for the corresponding irreversibly adsorbed adlayers shown in Figure 2A and B.

Interestingly, the bandwidth of the higher $-\theta_{CO}^{sat}$ feature in Figure 2B is unusually (even uniquely) narrow for a ν_{CO} band at in-situ electrochemical or even solvated metal−UHV interfaces,[11d,e] the full width at half-height, $\Delta\nu_{1/2}$, being 7.0 cm^{-1}. (Note that a 1−2 cm^{-1} spectrometer resolution setting was required in order to reliably determine this bandwidth.) The corresponding ν_{CO} band formed by CO dosing at 0.4 V is significantly broader, $\Delta\nu_{1/2} \approx 9.5$ cm^{-1}. The unusual narrowness of the ν_{CO} band in Figure 2B and its high A_i value (0.185 au cm^{-1}) combine to yield a remarkably large *peak* absorbance, $A_p = 0.020$ au. Indeed, converting this A_p value to the "percent absorption" (or "absorption intensity") scale, favored by UHV-based IRAS experimentalists,[26,27] yields a value of 4.5%. We shall return to the issue of absolute band intensities below.

Given that CO adsorption on Ir(110) also yields largely a single ν_{CO} band consistent with "atop" CO coordination, examination of the θ_{CO}-dependent spectra in comparison with those for Ir(111) is of interest. A typical set, for Ir(110) in 0.1 M $HClO_4$ at 0.35 V, obtained similarly to that for Ir(111) in Figure 1, is shown in Figure 3. The maximum CO coverage, $\theta_{CO}^{sat} = 1.15$, is obtained from the relative CO_2 A_p values on these two surfaces given that the metal atomic density on (unreconstructed) Ir(110) is 9.6×10^{14} atoms cm^{-2}. The overall θ_{CO}-dependent spectral fingerprint on Ir(110) is comparable to that on Ir(111), the ν_{CO} frequency blue-shifting substantially (by at least ca. 70 cm^{-1}) with increasing coverage, along with a progressive diminution in the bandwidth. However, extremely broad and asymmetric ν_{CO} bands are obtained at lower coverages, below 0.3. Similar θ_{CO}-dependent behavior, but not to the same extent, is observed for the Ir(110)−UHV system.[19] Slightly higher θ_{CO}^{sat} values, ca. 1.25, are also obtained for the electrochemical system upon CO dosing at potentials, 0.02 V, within the hydrogen region, again mirroring the behavior of Ir-(111).

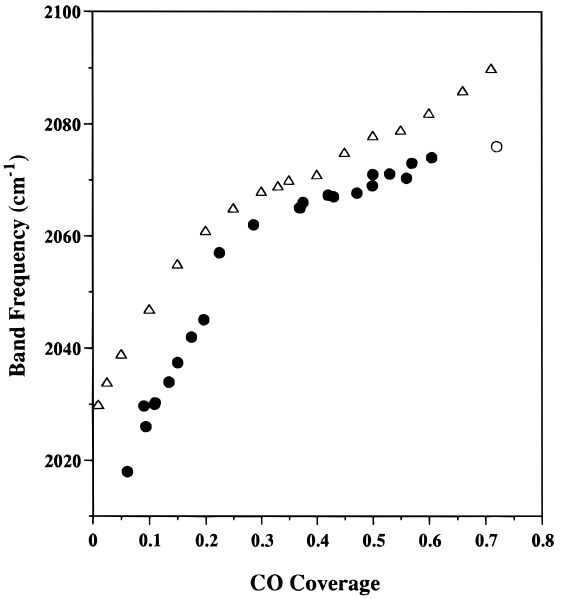

Figure 4. Peak frequency (cm^{-1}) of C−O stretching (ν_{CO}) band for CO dosed on Ir(111) plotted against the fractional CO coverage, θ_{CO}. Circles are for present aqueous electrochemical system, measured at 0.4 V (from Figures 1 and 2; open circle refers to spectrum in Figure 2B). Triangles are for corresponding Ir(111)−UHV interface at 300 K, extracted from data in ref 18.

As already noted, of central interest here is the detailed intercomparison of the θ_{CO}-dependent ν_{CO} spectral features on Ir(111) in the present aqueous electrochemical environment with corresponding IRAS results for the Ir(111)−UHV system, also obtained at ambient temperature (300 K), reported in ref 18. A logical starting point is to compare the peak frequencies, ν_{CO}^{p}, as a function of coverage. Figure 4 shows such a $\nu_{CO}^{p}-\theta_{CO}$ plot for the present electrochemical Ir(111)/CO system (circles), measured at 0.4 V vs SHE, compared with the corresponding

data for the Ir(111)−UHV interface at 300 K as reported by Lauterbach et al. in ref 18 (triangles). The filled circles refer to the irreversible CO adlayers dosed as well as measured at 0.4 V, whereas the sole open circle (for $\theta_{CO} = 0.72$) denotes the higher θ_{CO}^{sat} value attained by dosing instead at 0.05 V (Figure 2B). Comparison of the electrochemical and UHV-based $\nu_{CO}^{p}-\theta_{CO}$ plots reveals an intriguingly similar curved shape, the ν_{CO}^{p} values for the electrochemical system being ca. 10−20 cm^{-1} lower than for the UHV case throughout the accessible coverage range $0.05 \leq \theta_{CO} \leq 0.7$. Furthermore, this "displacement" of the two $\nu_{CO}^{p}-\theta_{CO}$ plots is approximately consistent with differences in the surface potential between the electrochemical and UHV-based interfaces, as deduced by the following analysis. (We have utilized similar analyses in earlier studies linking chemisorbate vibrational frequencies for electrochemical interfaces with both solvent-free and solvated metal−UHV systems; see, for example, refs 4−6, 8a, 11a, 12, and 16.)

One can relate the electrode potential for a given electrochemical interface, E (i.e., measured versus SHE or another reference electrode), with the corresponding work function, Φ, of the system (i.e., measured instead versus vacuum) by[28]

$$E = \Phi/e - E_k \quad (1)$$

where e is the electronic charge and E_k is the so-called "absolute potential" (versus vacuum) of the reference electrode. The precise value of E_k for the SHE (or any other reference electrode) remains controversial, estimates clustered around 4.45 and 4.85 V being deduced (and defended) by various means.[14a] Bearing this in mind, as a first step we can take an "average" value, 4.6 V (cf. refs 4, 8a, and 11a). We have obtained clear evidence, particularly from UHV "electrochemical modeling" studies, that the ν_{CO}^{p} values in a given adlayer in both electrochemical and UHV environments are dependent chiefly on Φ, rather than the specific nature of molecular coadsorbates such as the solvent.[3d,5,11a] Consequently, the ν_{CO}^{p} values at a given coverage in the Ir(111)−aqueous electrochemical system should equal those at the corresponding solvent-free Ir(111)−UHV interface when the Φ value for the former is adjusted to that for the latter surface, *provided* that the adlayer structures (CO binding sites, etc.) are the same in the two environments. [It should be borne in mind, however, that the (continuously adjustable) Φ value for the electrochemical interface will contain coupled contributions from the solvent dipoles and the electronic/ionic (double-layer) charges, so that the detailed electrostatic makeup of analogous metal−solution and metal−UHV systems will differ even when their Φ values are equal.[4a]]

The work function of clean Ir(111) is about 5.7 eV,[29] and saturation CO adsorption at 300 K increases Φ by 0.15 eV.[30] [The corresponding Φ and $\Delta\Phi$ values on Ir(110) are ca. 5.4[31] and 0.25 eV.[32]] The effective surface potentials of the Ir(111)/CO−UHV interface are therefore significantly higher than for the Ir(111)/CO aqueous system held at a fixed electrode potential, by an amount that increases somewhat with θ_{CO}. Given that the measured ν_{CO}^{p} values in Figure 4 refer to $E = 0.4$ V vs SHE, if we assume that $E_k \approx 4.6$ V we need to increase E by about 0.7 and 0.85 V at low and saturation θ_{CO} values, respectively, to attain the same surface potentials experienced by chemisorbed CO on Ir(111) in UHV. Since 0.4 V vs SHE is close to the electrode potential where CO electrooxidation commences, to obtain the required ν_{CO} frequency differences, $\Delta\nu_{CO}^{p}$, between the electrochemical and UHV systems due to surface-potential differences, it is necessary to extrapolate $\nu_{CO}^{p}-E$ data (obtained at various coverages) to higher potentials. A slight complication is that $\nu_{CO}^{p}-E$ data obtained by sweeping the potential, say, from 0.4 to 0 V and return, exhibit significant hysteresis, the $\nu_{CO}^{p}-E$ slopes obtained being 20−30% larger for the latter condition (cf. ref 7c). (This effect is probably related to the adlayer structural differences in the double-layer and hydrogen potential regions noted above.) However, taking the portion of the $\nu_{CO}^{p}-E$ data obtained exclusively in the "double−layer" region yields $d\nu_{CO}^{p}/dE$ values of about 25 cm^{-1} V^{-1} at θ_{CO}^{sat}, increasing to 50 cm^{-1} V^{-1} by $\theta_{CO} \sim 0.1$. Similar results were reported earlier.[7c] Utilizing these Stark-tuning slopes together with the differences in surface potential noted above yields predicted $\Delta\nu_{CO}^{p}$ values at low θ_{CO} of ca. 35 cm^{-1}, decreasing to 20 cm^{-1} at θ_{CO}^{sat}.

At least the former $\Delta\nu_{CO}{}^{p}$ estimate is significantly larger than that suggested by Figure 4, ca. 20 cm^{-1}. However, the reliability of the $\nu_{CO}^{p}-E$ extrapolation is most questionable at low θ_{CO}. Moreover, selecting a higher E_k value (4.9 V), as indicated by another Stark-tuning analysis of electrochemical and UHV-based infrared data,[12] diminishes the present $\Delta\nu_{CO}^{p}$ estimates to about 20 and 15 cm^{-1} at low and saturated θ_{CO} values, respectively. These values are indeed close to the observed θ_{CO}-dependent offsets between ν_{CO}^{p} in the electrochemical and UHV environments seen in Figure 4. Consequently, then, the observed ν_{CO}^{p} differences are likely to be due to primarily to surface-potential effects, rather than reflecting more intrinsic differences in chemisorbate bonding between the two environments. Essentially the same deduction is obtained from a similar analysis undertaken for the Ir(110)/CO system at intermediate and high CO coverages.

The second θ_{CO}-dependent spectral parameter of interest here is the integrated band intensity, A_i. Since A_i is both predicted and observed to have only a very weak dependence on the interfacial electrostatic field (and surface potential),[33] corrections for potential-induced differences in these parameters between the electrochemical and UHV-based interfaces are unnecessary. On the other hand, the infrared band intensities are dependent somewhat on both the external optical geometry employed for IRAS and the interfacial dielectric properties.[27,34,35] Both of these factors are significantly different between the electrochemical and UHV-based systems. While corrections can be made (see below), for the present purpose it is more useful to normalize the A_i values, most simply to that for a saturated CO adlayer. Figure 5 contains a plot of A_i versus θ_{CO} obtained for irreversibly adsorbed CO at the Ir(111)−aqueous electrochemical interface at 0.4 V (filled circles). The y-axis scale is in units of au cm^{-1}. The sole open circle is the corresponding high-coverage ($\theta_{CO} = 0.72$) point obtained for irreversibly adsorbed CO, also at 0.4 V, but formed instead by CO dosing at 0.05 V (cf. Figure 4). Given for comparison in Figure 5 is a $A_i-\theta_{CO}$ plot, extracted from Figure 4 of ref 18, for the corresponding Ir(111)−UHV system at 300 K (triangles). The latter A_i values have been normalized to the maximum absorbance observed for the irreversibly adsorbed electrochemical adlayers formed at 0.4 V. Analysis of the UHV-based ν_{CO} spectra (Figure 1 of ref 18; see erratum) yields an integrated intensity at saturation of 50.5% absorption cm^{-1}. This value is equivalent to 0.225 au cm^{-1} on the log absorbance scale employed here, slightly larger than the values obtained close to θ_{CO}^{sat} for the electrochemical interface (vide infra).

Comparison between the electrochemical and UHV-based $A_i-\theta_{CO}$ plots reveals a marked difference in morphology. While

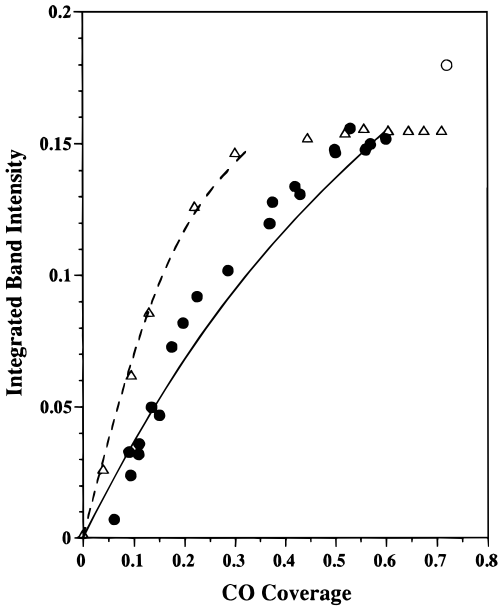

Figure 5. Integrated intensity of ν_{CO} band for CO dosed on Ir(111) in electrochemical and UHV-based environments plotted against θ_{CO}. Symbols as in Figure 4 (*y*-axis scale refers to integrated band absorbances, au cm^{-1}, in the electrochemical system.) Solid and dashed traces are obtained from numerical dipole-coupling analysis for the electrochemical and UHV systems, respectively (see text for details).

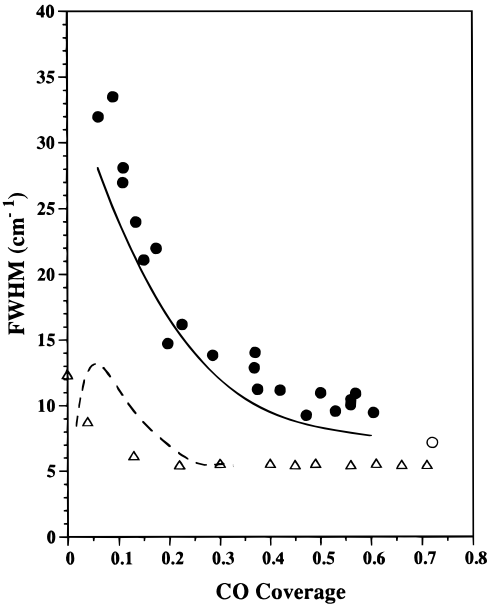

Figure 6. Line width (full width at half-maximum) of ν_{CO} band for CO dosed on Ir(111) in electrochemical and UHV-based environments plotted against θ_{CO}. Symbols as in Figure 4. Solid and dashed traces are obtained from numerical dipole-coupling analysis for the electrochemical and UHV systems, respectively (see text for details).

both plots are decidedly convex to the *y*-axis, the UHV-based A_i values rise rapidly and then are essentially *constant* for $\theta_{CO} > 0.3$.[18] The electrochemical A_i values instead increase monotonically with a lower slope toward higher θ_{CO}. The same overall trend is seen if one includes the higher-θ_{CO} point (open circle) obtained by CO dosing within the hydrogen region, at 0.05 V (Figure 5). Qualitatively similar differences in the $A_i-\theta_{CO}$ plots are also observed on Ir(110) between the UHV-based[29] and electrochemical systems. The implications of this differing behavior to the elucidation of solvation effects upon adlayer structure are discussed below.

The third θ_{CO}-dependent spectral parameters of significance here is the line width of the ν_{CO} bands, especially given that infrared band broadening is commonly engendered by solvation. Figure 6 contains a plot of the bandwidth, expressed as the "full width at half-maximum", $\Delta\nu_{1/2}$, versus θ_{CO} for the Ir(111)/CO−electrochemical interface. As before (Figures 4 and 5), the filled circles refer to the adlayers at 0.4 V formed by CO dosing at the same potential, and the open circle to the higher-coverage saturated adlayer formed instead at 0.05 V. Similarly to some other aqueous electrochemical adlayers (e.g., Pt(111)/CO[17]), $\Delta\nu_{1/2}$ is seen to decrease markedly toward higher θ_{CO}. The corresponding plot for the Ir(111)/CO−UHV system at 300 K, taken from Figure 5 of ref 18, is shown as triangles in Figure 6. Analogously to the $A_i-\theta_{CO}$ behavior (Figure 5), the UHV $\Delta\nu_{1/2}$ values are essentially θ_{CO}-independent for $\theta_{CO} > 0.3$. The UHV-based bandwidths are also smaller at all coverages than the corresponding electrochemical $\Delta\nu_{1/2}$ values, especially at low θ_{CO}, although the latter converge toward the former as θ_{CO} approaches saturation (Figure 6). An analysis of the ν_{CO} band shapes for the electrochemical system revealed a better fit to a Lorentzian rather than a Gaussian shape, at least for $\theta_{CO} \geq 0.3$, although a low-frequency "tail" is evident at all coverages. This tail becomes more prominent toward lower coverages, for $\theta_{CO} < 0.4$ (Figure 1). A similar ν_{CO} band shape asymmetry is seen in the UHV-based system at low coverages, although a narrow Lorentzian-shaped band is evident for $\theta_{CO} \geq 0.3$.[18] A unified interpretation of these $\Delta\nu_{1/2}-\theta_{CO}$ trends, along with the corresponding $\nu^p_{CO}-\theta_{CO}$ and $A_i-\theta_{CO}$ behavior, will now be undertaken.

Discussion

The striking parallel in the $\nu^p_{CO}-\theta_{CO}$ behavior observed on the aqueous electrochemical and UHV-based Ir(111) surfaces (Figure 4), especially after correcting for the difference in θ_{CO}-dependent surface potentials (vide infra), provides a clear indication of the close similarity in chemisorbate binding encountered in these two environments. There are inevitable uncertainties, however, not only in the precise surface-potential differences but also in the CO coverages themselves. While the combined coulometric−spectrophotometric analysis employed to evaluate θ_{CO} at the electrochemical interface (vide supra) should yield reliable values (±5%),[25] the situation is perhaps not as clear-cut in the UHV system. The UHV coverages are calibrated by noting the point (corresponding to $\theta_{CO} = {}^1/_3$) where the $(\sqrt{3} \times \sqrt{3})R30°$ low-energy diffraction (LEED) pattern is sharpest.[18] Nevertheless, it is reasonable to presume that the θ_{CO} scales for the electrochemical and UHV systems are approximately concordant (say, within 10%).

The nonlinear $\nu^p_{CO}-\theta_{CO}$ behavior observed at the Ir(111)−UHV interface was analyzed in terms of a dipole−dipole coupling model, utilizing $C^{18}O/C^{16}O$ isotopic mixtures to separate the total θ_{CO}-induced ν^p_{CO} shifts into dynamic coupling, $\Delta\nu_D$, and static ("chemical") contributions, $\Delta\nu_C$.[18] Most of the overall ν^p_{CO} blue shift was found to arise from the $\Delta\nu_D$ component, the $\Delta\nu_C$ term being smaller (~10 cm^{-1}) and almost θ_{CO}-independent.[18] Comparing the observed $\Delta\nu_D-\theta_{CO}$ (and hence $\nu^p_{CO}-\theta_{CO}$) dependence with the predictions of a conventional dipole-coupling model yielded a better fit by taking into account the likely effects of nonrandom adsorption (CO clustering) at higher coverages, as also suggested from LEED data.[18] Unfortunately, the high cost of $C^{18}O$ prevented such an isotopic analysis from being undertaken for the present electrochemical system. (Experiments using the cheaper isotope

^{13}CO yielded an insufficient wavenumber separation between $^{13}CO/^{12}CO$ band partners.[7c]) Nonetheless, the similarly nonlinear $\nu^{p}_{CO}-\theta_{CO}$ functionality observed for the Ir(111)−aqueous interface (Figure 4) suggests strongly that the θ_{CO}-dependent dipole coupling does not differ greatly from that for the UHV system (vide infra).

Consideration of the corresponding band absorbance-coverage ($A_i-\theta_{CO}$) plots (Figure 5), however, provides clear evidence for the role of chemisorbate solvation in altering the electrochemical infrared properties. Two differences between the $A_i-\theta_{CO}$ behavior of the electrochemical and UHV-based systems, evident at low and high CO coverages, are informative and are discussed in turn. First, the relative $A_i-\theta_{CO}$ slope observed for the electrochemical interface at low θ_{CO} (<0.2) is significantly (ca. 30%) smaller than obtained in UHV (Figure 5). (Admittedly, the extent of this slope difference depends somewhat on the high-θ_{CO} A_i value used for normalization, a ca. 10% greater dissimilarity than that shown in Figure 5 resulting if the A_i values at $\theta_{CO} \approx 0.7$ are set to be equal.)

Interestingly, such a difference in the initial $A_i-\theta_{CO}$ slope is anticipated from dielectric screening of the C−O dynamic dipole by surrounding solvent molecules.[11d,12,36] Physically, the effect involves an attenuation of the chemisorbate dynamic dipole moment (or "vibrational polarizability" α_v), and hence the infrared band intensity, by the polarizable electron cloud contained in adjacent coadsorbates.[37−39] Consequently, the degree of band attenuation will depend on the *electronic* polarizability, α_e, of the surrounding coadsorbate species. In practice, this screening effect has been considered chiefly in the context of dipole-coupling treatments for pure chemisorbate layers in UHV.[37−39] Infrared band attenuation will occur here via dielectric screening with surrounding chemisorbate oscillators, so that the effect is negligible at very low θ_{CO} but increases progressively toward higher θ_{CO}, thereby yielding nonlinear $A_i-\theta_{CO}$ profiles.[37−39]

A well-known formula, derived from a dielectric-screening analysis for pure chemisorbate layers,[37] is

$$A_i \propto \alpha_v(1 + \alpha_e \tilde{U})^{-2} \qquad (2)$$

where α_v and α_e are the vibrational and electronic polarizabilities of the chemisorbate, and $\tilde{U}$ is the lattice-sum term that depends on the chemisorbate spatial positions (packing density).[37−39] Equation 2 has been utilized previously to estimate roughly the degree of band intensity attenuation at low coverages by (close-packed) solvent by replacing the chemisorbate α_e (about 2.5 Å^3 [37]) with the solvent electronic polarizability.[11d] This simplified treatment predicts an absorbance attenuation factor at low oscillator coverage induced by interfacial solvation, A_i^s/A_i^0 [$=(1 + \alpha_e \tilde{U})^{-2}$], of ca. 2-fold with water, for which $\alpha_e = 1.5$ Å^3.[11d,40] (Distinctly larger attenuation factors, i.e., smaller A_i^s/A_i^0 values, are predicted for a number of nonaqueous species, for example acetone and especially benzene, arising from their greater electronic polarizabilities, ca. 6.5 and 10.5 Å^3.[11d]) While crude, the predictions are roughly in accordance with IRAS data for the low-temperature solvation of CO and NO adlayers on Pt(111) in UHV[11c,12] (vide infra).

A related analytical formalism accounting for dielectric screening of chemisorbate vibrations by surrounding molecules (or atoms) has been described,[42] which yields at low oscillator coverage and high coadsorbate dosages (surrounding the former by hexagonal close packing) the limiting expression

$$A_i^s/A_i^0 = (1 - 6\alpha_e d^{-3})^2 \qquad (3)$$

where α_e is again the coadsorbate polarizability and d is the (van der Waals) oscillator−coadsorbate separation. (Modified, more complicated, formulas have been deduced for intermediate oscillator coverages.[42]) Assuming that $d \sim 3$ Å (the effective "diameter" of both water and chemisorbed CO) yields a predicted hydration-induced intensity attenuation factor (A_i^s/A_i^0) of, again, about 2-fold.

These predicted attenuation factors are comparable to, if somewhat larger than, the experimental value deduced from Figure 5 (ca 1.3−1.5). Interpretation of our earlier UHV-based measurements of solvent-induced infrared attenuation for low-coverage CO adlayers on Pt(111) is complicated by alterations in chemisorbate binding geometry.[11d] However, this obfuscating factor is apparently absent for hydration of NO adlayers on Pt(111).[12] Interestingly, hydration of low NO coverages also yields about a 1.5-fold decrease in the N−O stretching (ν_{NO}) band intensity (as deduced from spectra in Figure 4A of ref 12).

One would expect the degree of ν_{CO} (or ν_{NO}) band intensity diminution arising from surface solvation to decline toward intermediate and high chemisorbate coverages, as the nearest neighbors are composed decreasingly of solvent and increasingly of chemisorbate molecules. However, coadsorbed CO should act to screen the C−O dynamic dipoles *more* effectively than water in view of its higher effective electronic polarizability, ca. 2.5 Å^3.[37] Thus, for close-packed CO, from eq 2 one typically predicts that[11d] $A_i^0/A_i^s \sim 3$. Consequently, then, we anticipate on this basis that the $A_i-\theta_{CO}$ plot for random CO adsorption on Ir(111) in aqueous solution would be somewhat curved, the slopes decreasing by about 2-fold toward high coverages. Indeed, such a morphology is clearly observed in Figure 5, the $A_i-\theta_{CO}$ slopes declining by this factor from the low-θ_{CO} (≤ 0.2) to high-θ_{CO} (>0.35) regions.

We have also undertaken a more quantitative spectral analysis involving numerical simulations based on dipole−dipole coupling models. Such calculations were motivated originally by the need to interpret band "intensity-transfer" effects observed in CO/NO coadsorbate mixtures on Ir(111) and (110).[9b,c] Since they also provide insight into the θ_{CO}-dependent band absorbance and bandwidth behavior observed in the electrochemical and UHV environments, some salient findings are also given here. The numerical dipole−dipole analysis was undertaken as follows. (See refs 9c and 10b for further details.) The chemisorbate layer was modeled as a large (100−300 molecule) hexagonal array with $\theta = 0.6$, the sites being filled randomly with CO or water molecules so to yield the desired θ_{CO} value. (Other packing arrangements yielded similar results.) The ν_{CO} band frequencies and relative intensities were calculated as described in ref 10b, following essentially the method of Greenler and co-workers[43] with periodic boundary conditions. The chemisorbate dipoles were presumed to lie 0.8 Å above the image plane.[10b] The required CO vibrational polarizability, $\alpha_v = 0.41$ Å^3, was selected by fitting the simulated $\nu^{p}_{CO}-\theta_{CO}$ results to the experimental data in Figure 5, so to reproduce approximately the shape and overall θ_{CO}-induced frequency blue shifts. The electronic polarizability values, α_e, selected for CO and water were again 2.5 and 1.5 Å^3, respectively.[40]

The solid $A_i-\theta_{CO}$ trace included in Figure 5, normalized to the maximum experimental A_i value, was extracted from this numerical analysis. While the calculated curve does not yield a precise fit to the experimental points (filled circles), it nonetheless also exhibits a decreasing slope toward higher coverages. As already noted, this behavior reflects the predicted enhancement of dielectric screening of the dynamic C−O dipole

as these oscillators are surrounded increasingly by other CO molecules rather than water molecules.

Significantly, the numerical analysis is also able to describe the markedly different experimental $A_i-\theta_{CO}$ curve obtained in the absence of coadsorbed water, i.e., in UHV. The calculated trace (dashed line) is shown in comparison with the experimental UHV data (open triangles) in Figure 5, with the former again normalized to the maximum (high-θ_{CO}) observed A_i value. This predicted trace was obtained from a similar numerical analysis as above (using a slightly lower α_v value for CO, 0.37 Å^3, suggested by fitting to the UHV $\nu^p_{CO}-\theta_{CO}$ data, Figure 4). More significantly, however, over the θ_{CO} range 0 to $^1/_3$, the CO was filled into atop sites randomly as before, but limiting the nearest distance between (atop) CO's to 4.7 Å, rather than the "nearest-neighbor" value, 3.5 Å, employed for the electrochemical simulations. The former corresponds to the $(\sqrt{3} \times \sqrt{3})R30°$ ordered adlayer structure which is observed by low-energy diffraction (LEED) for $\theta_{CO} = {}^1/_3$.[18,44] (The appearance of this LEED pattern at lower coverages indicates that some "ordered" CO islands are also formed for $\theta_{CO} < {}^1/_3$.[18]) As noted in ref 18, dipole-coupling calculations undertaken for higher θ_{CO}, up to saturation ($\approx$0.7) are complicated by the nonrandom adsorption evident from LEED. A simulation was nonetheless undertaken here for the coverage (7/12) corresponding to the ordered $(2\sqrt{3} \times \sqrt{3})$ structure, again with molecules adsorbed in equivalent sites. This yielded a A_i value closely similar to that calculated for $\theta_{CO} = {}^1/_3$, in agreement with experiment (Figure 5). The calculated (dashed) line shown in Figure 5 is normalized to the experimental A_i value at $\theta_{CO} = 7/12$. Such θ_{CO}-insensitive, or even peaked, $A_i-\theta_{CO}$ behavior is often seen for higher θ_{CO} values at metal−UHV interfaces, due to the enhanced dielectric screening from nearby CO's offsetting the increase in oscillator density.[39]

Comparison with the experimental UHV-based data (open triangles, Figure 5) shows that the calculated $A_i-\theta_{CO}$ curve reproduces well the observed shape, featuring a sharp A_i rise at low coverages up to $\theta_{CO} \sim {}^1/_3$. Most significantly for the present purposes, the simulation accounts for the markedly different $A_i-\theta_{CO}$ dependences observed in the UHV and aqueous electrochemical environments, including the smaller $A_i-\theta_{CO}$ slope at low coverages for the latter. Admittedly, it is uncertain on this basis whether some milder degree of chemisorbate ordering at intermediate coverages also occurs at the electrochemical interface. Such partial ordering may be responsible for the positive deviations of the experimental $A_i-\theta_{CO}$ points (solid circles) above the calculated curve (solid trace, Figure 5). In addition, chemisorbate solvation may influence the adlayer dielectric properties at higher CO coverages. Thus, the solvent can be imagined as partly penetrating the CO adlayer interstices even at near-saturated θ_{CO} values, screening somewhat the oscillator dipoles and possibly limiting chemisorbate island formation. A plausible additional factor is dielectric screening engendered by "second-layer" solvent molecules on top of the chemisorbate monolayer. Nevertheless, water addition to a saturated NO layer on Pt(111) in UHV at 100 K yields essentially (within ca. 10%) no alteration in A_i for the ν_{NO} band (as discerned from Figure 3A of ref 12), even though the ν_{NO} frequency is red-shifted to an extent consistent with the observed water-induced Φ change.[12]

Further insight into the importance of interfacial hydration on the local chemisorbate environment under these circumstances is seen by examining the θ_{CO}-dependent ν_{CO} bandwidths, $\Delta\nu_{1/2}$, plotted in Figure 6. Most pointedly, while the Ir(111)−UHV interface yields a coverage-independent $\Delta\nu_{1/2}$ value, ca. 5 cm^{-1}, for $\theta_{CO} > 0.3$, mirroring the $A_i-\theta_{CO}$ morphology, the corresponding electrochemical $\Delta\nu_{1/2}$ values decrease continuously with increasing θ_{CO} up to saturation. At first sight, the larger bandwidths obtained in the aqueous electrochemical environment might be attributed to inhomogeneous line broadening associated with chemisorbate hydration. However, the observation of essentially Lorentzian, rather than Gaussian, band shapes argues against this possibility. Moreover, we have observed similar θ_{CO}-dependent $\Delta\nu_{1/2}$ values (and band shapes) on Ir(111) in aqueous solution for CO intermixed with coadsorbed NO as well as with water.[9c]

A more likely explanation for the electrochemical $\Delta\nu_{1/2}-\theta_{CO}$ behavior is evident, however, from the dipole-coupling simulations. The solid trace in Figure 6 shows the θ_{CO}-dependent $\Delta\nu_{1/2}$ values extracted from the simulated spectra obtained as outlined above, selecting an "intrinsic" (saturated-θ_{CO}) value of 8 cm^{-1} to match this experimental limit. The calculated curve is seen to provide a reasonable fit to the experimental data (filled circles, Figure 6). The progressive increases in the simulated $\Delta\nu_{1/2}$ values toward lower θ_{CO} reflect "stochastic broadening", arising physically from statistically random variations in the local CO coverages.[45] Microscopic regions where the chemisorbate spacing is smaller than average (such as CO's where one or more nearest-neighbor sites are occupied) will provide blue-shifted C−O oscillator frequencies due to enhanced dipole−dipole coupling. Furthermore, although constituting a minority of the CO ensemble at low θ_{CO}, these oscillator components will exert a disproportionately large influence on the resulting ν_{CO} band as a result of "intensity transfer"[39a] from spatially juxtaposed but less blue-shifted components associated with microscopically lower coverage (i.e., more "isolated") CO's.[9c] Consequently, the simulated ν_{CO} bands are asymmetric at smaller (macroscopic) θ_{CO} values, exhibiting a pronounced "tail" toward lower wavenumbers which is chiefly responsible for the enhanced $\Delta\nu_{1/2}$ values. This behavior is closely similar to the θ_{CO}-dependent appearance of the experimental ν_{CO} spectra (Figure 1).

The bandwidth narrowing seen toward higher θ_{CO} (Figure 1; filled circles, Figure 6) can also be understood on this basis from the progressively greater extent of "intensity bias" (via intensity transfer) toward the most blue-shifted oscillator spatial patches as the overall CO packing density and hence the extent of dipole−dipole coupling increases. Such coupling-induced "band narrowing" has been discussed in detail.[46] While this stochastic-broadening dipole-coupling model is largely successful in describing the electrochemical $\Delta\nu_{1/2}-\theta_{CO}$ behavior, it is also possible that some degree of solvation-induced inhomogeneous band broadening is present. (This effect arises from microscopic fluctuations in the chemisorbate solvation environment.[47,48]) Such a component may be responsible for the ca. 2-fold larger $\Delta\nu_{1/2}$ values observed in the electrochemical versus the UHV system at near-saturated θ_{CO} values (Figure 6). Indeed, significant (ca. 2−3-fold) band broadening has been observed for saturated (or near-saturated) CO and NO layers on Pt(111) upon solvent addition at low temperature ($\sim$100 K) in UHV.[11,12] Such effects may again arise from solvation of the chemisorbate oxygen by second-layer solvent dipoles.

Given the latter findings, the observation of a ν_{CO} band for a "compressed saturated" CO adlayer ($\theta_{CO} = 0.72$) at the Ir(111)−aqueous interface (Figure 2B) having a line width, 7 cm^{-1}, approaching that for the *solvent-free* Ir(111)−UHV system, 5 cm^{-1}, is noteworthy. One can surmise that the electrochemical CO adlayer is then sufficiently compressed to eliminate water from any remaining adlattice interstices, thereby

attaining more homogeneity. Indeed, the (2 × 2)-3CO adlayer on Pt(111) in aqueous media,[10] which is similarly compressed ($\theta_{CO} = 0.75$), also exhibits a narrow atop ν_{CO} feature, $\Delta\nu_{1/2} \approx 9$ cm^{-1}, as deduced from Figure 8 of ref 10a. However, such line narrowing is anticipated even for inhomogeneous adlayers if the dipole−dipole coupling is sufficiently strong, since then intensity transfer will cause the absorption band shape to reflect chiefly the blue (highest-wavenumber) end of the oscillator frequency distribution.[45] Significantly, such strong band intensity transfer is indeed prevalent in highly compressed adlayers, as has been demonstrated for the Pt(111) (2 × 2)-3CO structure.[10b] The observed preferential formation of such highly compressed CO adlayers on Ir(111) [and Pt(111)[10]] at lower electrode potentials (vide supra) is consistent with the stronger metal−CO bonding occurring under such conditions, as also reflected in the observed increases in surface−adsorbate stretching frequencies, ν_{M-CO}.[49] The especially strong atop-CO binding observed on iridium is also in harmony with the high ν_{M-CO} values (ca. 500 cm^{-1}) observed on this metal.[49]

It remains to consider the distinctly different $\Delta\nu_{1/2}-\theta_{CO}$ dependence observed for the UHV system (open triangles, Figure 6). Numerical simulations were undertaken in the manner outlined above, taking the "intrinsic" line width as 5 cm^{-1} so to match the experimental high−θ_{CO} value.[18] (The likely factors affecting this line width, including electron−hole pair lifetime broadening, are discussed in ref 18.) At very low coverages, $\theta_{CO} < 0.2$, calculated $\Delta\nu_{1/2}$ values were obtained, ca. 8−12 cm^{-1}, that roughly match the experimental UHV-based data. The 2−3-fold smaller $\Delta\nu_{1/2}$ values than calculated (and also measured) for the electrochemical system are due simply to the larger assumed minimum CO−CO separation (4.7 Å) in the former case, thereby restricting the occurrence of blue-shifted "local oscillator" components. The $\Delta\nu_{1/2}-\theta_{CO}$ curve calculated in this fashion is the dashed trace in Figure 5. While the simulations account for the observed θ_{CO}-independent $\Delta\nu_{1/2}$ values for $\theta_{CO} > 0.2$, the "peaked" $\Delta\nu_{1/2}-\theta_{CO}$ shape predicted at low θ_{CO} is not matched by experiment. However, simulated $\Delta\nu_{1/2}-\theta_{CO}$ plots that are closely similar to the experimental behavior were obtained from calculations assuming a degree of nonrandom low-θ_{CO} adsorption, so to yield small ($\sqrt{3} \times \sqrt{3}$) islands. As mentioned above, such island formation is indeed suggested from low-θ_{CO} LEED data.[18,44]

Overall, then, the marked dissimilarities observed experimentally for the θ_{CO}-dependent ν_{CO} bandwidths as well as absorbances in the electrochemical and UHV environments can be ascribed to solvent-induced difference in the chemisorbate spatial distributions at both low and intermediate coverages. The presence of the solvent generally appears to yield more statistically random CO adsorption, removing the tendency to form ($\sqrt{3} \times \sqrt{3}$) or other local superstructures at intermediate coverages. While the underlying reasons for this behavior are not as clear-cut as, for instance, solvent-induced dielectric screening, chemisorbate hydration should yield significant changes in (most likely attenuation of) CO−CO lateral interactions.

One last point of comparison between the Ir(111)−UHV and Ir(111)−aqueous interfaces is worthy of mention here. While we have normalized the integrated band intensities in these two environments in constructing in Figure 5, in principle the *measured absolute* A_i values could usefully be compared given a knowledge of the optical properties, including geometries, of the IRAS configurations employed. While seldom discussed in the literature, such a comparison for the present surface−chemisorbate system is feasible. There are two primary optical factors that are anticipated to yield "intrinsic" differences in A_i between the in-situ electrochemical and UHV environments. First, the effective angle of incidence, ϕ, for the incoming beam (versus the surface normal) can be arranged in the UHV system to be close to the angle, ca. 85°, desired for optimizing the p-polarized electric field vector, and hence maximizing A_i.[27,35] (This was apparently the case in ref 18.) In the electrochemical IRAS experiment, however, the effective ϕ value is constrained somewhat by the need to pass the beam through an optical window, forming the solution thin layer in front of the metal surface. As is conventional, our window consists of a 60° beveled CaF_2 prism so to minimize refraction at the initial gas−window interface. With aqueous solution in the thin layer, this arrangement yields a smaller effective ϕ value at the metal surface, about 70°.[50] This factor, taken alone, should yield A_i values that are significantly (ca. 4-fold) smaller for the electrochemical versus the UHV surface, due to a less optimal ϕ value.[51]

A second, compensating, factor to be considered, however, is that the refractive index of the region lying just beyond the chemisorbate layer at the aqueous electrochemical interface is higher (ca. 1.3) than in the UHV system (1.0). This effect will generate a larger "effective ϕ" angle within the chemisorbate layer for a given *external* ϕ value in the electrochemical versus the UHV system. While such calculations are only approximate (in the classical limit),[34,35] this factor can at least partly compensate for the smaller external ϕ values obliged for the electrochemical IRAS experiment.

Interestingly, the A_i value for the "saturated" CO adlayer ($\theta_{CO} \approx 0.7$) measured at the Ir(111)−aqueous interface, 0.185 au cm^{-1}, is only marginally smaller than that deduced for the corresponding adlayer in UHV, 0.23 au cm^{-1}.[52] It therefore appears that there is no substantial infrared band attenuation brought about by the different optical geometry obliged for the thin-layer electrochemical interface. Of course, as already mentioned the solvent-induced band broadening commonly encountered in electrochemical systems will tend to diminish the *peak* absorbances, so that band *detection* can be impaired even if the integrated intensity is not greatly altered by local environmental factors. Given the practical significance of this issue for electrochemical IRAS, more comprehensive comparisons along these lines for "common chemisorbate structures" in metal−solution and UHV-based systems would appear to be worthwhile.

Concluding Remarks

At least on a semiquantitative level, the various physical influences exerted by the aqueous double-layer environment on the coverage-dependent infrared spectroscopic properties of the CO chemisorbate on Ir(111) appear to be reasonably well understood. Significantly, the marked differences in θ_{CO}-dependent ν_{CO} absorbances and band shapes between the electrochemical and UHV-based systems, as well as the relationship between peak frequencies, can be accounted for in terms of chemisorbate solvation and related effects. The apparently single-site CO binding geometry on Ir(111), together with large θ_{CO}-dependent adsorbate−adsorbate interactions, endow the surface with near-ideal properties for exploring such effects in the welcome absence of obfuscating "chemical" influences. The role of the solvent in screening electronically the chemisorbate dynamic dipole moment, and hence attenuating the infrared band intensity at lower coverages as observed here, should be a ubiquitous effect for electrochemical systems. Indeed, such dielectric screening should be present for *any*

intermixed coadsorbate system, although it may be overshowed by other effects, such as band "intensity transfer" when the coadsorbates feature comparable oscillator frequencies.[37,38] [We describe elsewhere an instructive example of intensity-transfer effects for the Ir(111)/CO−aqueous and related interfaces in the presence of coadsorbed NO.[9b,c]]

In the present Ir(111)/CO electrochemical system, another role of intensity-transfer effects is apparently manifested in the progressively larger bandwidths seen toward lower CO, consistent with statistical fluctuations in the local CO oscillator density ("stochastic line broadening"). The smaller extent of such band-broadening effects in the UHV-based system, together with the coverage-insensitive $\Delta\nu_{1/2}$ and A_i values for $\theta_{CO} > 0.25$ or so, are indicative of nonrandom CO adsorption, including local island formation. These differences clearly implicate a role of solvation in altering, and probably attenuating, the local lateral chemisorbate interactions at low and intermediate coverages. The manner in which the solvent modifies the chemisorbate vibrational properties at higher CO coverages is less clear-cut, although the "secondary" solvation layer covering the adlattice may still influence the band intensity and line width. Lastly, while surface solvation commonly yields large (1−2 eV) decreases in the metal work function, Φ, and hence *by itself* can substantially alter the chemisorbate stretching frequency (by ca. 30−70 cm^{-1}),[11c] the *net* effects upon the ν_{CO} band frequency *at a given* Φ *value* engendered by coupled dipolar solvation/double-layer charging are seen to be small or even negligible. This finding is consistent with the behavior observed on other transition-metal surfaces.[4−7,10−12]

Acknowledgment. C.T. is grateful to the National Science Council of Taiwan for financial support. This work has also been supported by the U.S. National Science Foundation.

References and Notes

(1) For example: (a) Weaver, M. J. *J. Phys. Chem.* **1996**, *100*, 13079. (b) Weaver, M. J.; Gao, X. *Annu. Rev. Phys. Chem.* **1993**, *44*, 459.

(2) For example: Hubbard, A. T. *Chem. Rev.* **1988**, *88*, 63.

(3) For reviews, see: (a) Nichols, R. J. In *Adsorption of Molecules at Electrodes*; Lipkowski, J., Ross, P. N., Eds.; VCH Publishers: Weinheim, 1992; Chapter 7. (b) Iwasita, T.; Nart, F. C. In *Advances in Electrochemical Science and Engineering*, Gerischer, H., Tobias, C. W., Eds.; VCH Publishers: Weinheim, 1995; Vol. 4, p 123. (c) Korzeniewski, C.; Severson, M. W. *Spectrochim. Acta* **1995**, *51A*, 499. (d) Weaver, M. J.; Zou, S. In *Spectroscopy for Surface Science*; Advances in Spectroscopy, Vol. 26; Clark, R. J. H., Hester, R. E., Eds.; Wiley: Chichester, 1998; Chapter 5.

(4) (a) Chang, S.-C.; Weaver, M. J. *J. Phys. Chem.* **1991**, *95*, 5391. (b) Chang, S.-C., Weaver, M. J. *Surf. Sci.* **1990**, *238*, 142.

(5) Villegas, I., Weaver, M. J. *J. Phys. Chem. B* **1997**, *101*, 10166.

(6) (a) Chang, S.-C.; Jiang, X.; Roth, J. D.; Weaver, M. J. *J. Phys. Chem.* **1991**, *95*, 5378. (b) Jiang, X.; Weaver, M. J. *Surf. Sci.* **1992**, *275*, 237.

(7) (a) Gómez, R.; Weaver, M. J. *J. Phys. Chem. B* **1998**, *102*, 3754. (b) Gómez, R.; Weaver, M. J. *Langmuir* **1998**, *14*, 2525. (c) Jiang, X.; Chang, S.-C.; Weaver, M. J. *J. Phys. Chem.* **1991**, *95*, 6453.

(8) (a) Zou, S.; Gómez, R.; Weaver, M. J. *Surf. Sci.* **1998**, *399*, 270. (b) Zou, S.; Weaver, M. J. Manuscript in preparation.

(9) (a) Tang, C.; Zou, S.; Weaver, M. J. *Surf. Sci.* **1998**, *412/413*, 344. (b) Weaver, M. J.; Tang, C.; Zou, S.; Severson, M. W. *J. Chem. Phys.* **1998**, *109*, 4135. (c) Tang, C.; Zou, S.; Severson, M. W.; Weaver, M. J. *J. Phys. Chem. B*, in press.

(10) (a) Villegas, I.; Weaver, M. J. *J. Chem. Phys.* **1994**, *101*, 1648. (b) Severson, M. W.; Stuhlmann, C.; Villegas, I.; Weaver, M. J. *J. Chem. Phys.* **1995**, *103*, 9832.

(11) For example: (a) Villegas, I.; Weaver, M. J. *J. Phys. Chem. B* **1997**, *101*, 5842. (b) Kizhakevariam, N.; Villegas, I.; Weaver, M. J. *J. Phys. Chem.* **1995**, *99*, 7677. (c) Kizhakevariam, N.; Villegas, I.; Weaver, M. J. *Langmuir* **1995**, *336*, 37. (d) Kizhakevariam, N.; Villegas, I.; Weaver, M. J. *Langmuir* **1995**, *11*, 2777. (e) Kizhakevariam, N.; Jiang, X.; Weaver, M. J. *J. Chem. Phys.* **1994**, *100*, 6750.

(12) Villegas, I.; Gómez, R.; Weaver, M. J. *J. Phys. Chem.* **1995**, *99*, 14832.

(13) (a) Sass, J. K.; Bange, K. *ACS Symp. Ser.* **1988**, *378*, 54. (b) Sass, J. K.; Bange, K.; Döhl, R.; Piltz, E.; Unwin, K. *Ber. Bunsen-Ges. Phys. Chem.* **1984**, *88*, 354.

(14) (a) Wagner, F. T. In *Structure of Electrified Interfaces*; Lipkowski, J., Ross, P. N., Eds.; VCH Publishers: New York, 1993; Chapter 9. (b) Stuve, E. M.; Kizhakevariam, N. *J. Vac. Sci. Technol. A* **1993**, *11*, 2217.

(15) (a) Lambert, D. K. *Electrochim. Acta* **1996**, *41*, 623. (b) Lambert, D. K. *J. Chem. Phys.* **1988**, *89*, 3847.

(16) Weaver, M. J. *Appl. Surf. Sci.* **1993**, *67*, 147.

(17) Chang, S.-C.; Weaver, M. J. *J. Chem. Phys.* **1990**, *92*, 4582.

(18) Lauterbach, J.; Boyle, R. W.; Schick, M.; Mitchell, W. J.; Meng, B.; Weinberg, W. H. *Surf. Sci.* **1996**, *350*, 32. Also see erratum in: *Surf. Sci.* **1996**, *366*, 228.

(19) Lyons, K. J.; Xie, J.; Mitchell, W. J.; Weinberg, W. H. *Surf. Sci.* **1995**, *325*, 85.

(20) Corrigan, D. S.; Weaver, M. J. *J. Electroanal. Chem.* **1988**, *241*, 143.

(21) Gómez, R.; Weaver, M. J. *J. Electroanal. Chem.* **1997**, *435*, 205.

(22) Motoo, S.; Furuya, N. *J. Electroanal. Chem.* **1984**, *181*, 301.

(23) Hoshi, N.; Uchida, T.; Mizinwa, T.; Tori, Y. *J. Electroanal. Chem.* **1995**, *381*, 261.

(24) Weaver, M. J.; Chang, S.-C.; Leung, L.-W. H., Jiang, X.; Rubel, M.; Szlarzyk, M.; Zurawski, D.; Wieckowski, A. *J. Electroanal. Chem.* **1992**, *327*, 247.

(25) Gómez, R.; Feliu, J. M.; Aldaz, A.; Weaver, M. J. *Surf. Sci.* **1998**, *410*, 48.

(26) Schweizer, E.; Persson, B. N. J.; Tüshaus, M.; Hoge, D.; Bradshaw, A. *Surf. Sci.* **1989**, *213*, 49.

(27) Bradshaw, A. M.; Schweizer, E. In *Spectroscopy of Surfaces*; Clark, R. J. H., Hester, R. E., Eds.; Wiley: Chichester, 1988; Vol. 16, Chapter 8.

(28) (a) Trasatti, S. *J. Electroanal. Chem.* **1983**, *150*, 1; **1982**, *139*, 1. (b) Trasatti, S. *Surf. Sci.* **1995**, *335*, 1.

(29) Nieuwenhuys, B. E.; Sachtler, W. M. H. *Surf. Sci.* **1974**, *45*, 513.

(30) Küppers, J.; Plagge, A. *J. Vac. Sci. Technol.* **1976**, *13*, 259.

(31) While lower values of Φ for clean Ir(110) have been reported,[29] the present estimate appears to be more reasonable in view of the Φ values for the (111) and (100) planes also quoted in ref 29.

(32) Taylor, J. L.; Ibbotson, D. E.; Weinberg, W. H. *J. Chem. Phys.* **1978**, *69*, 4298.

(33) Lambert, D. K. *J. Chem. Phys.* **1991**, *94*, 6237.

(34) Greenler, R. G. *J. Chem. Phys.* **1966**, *44*, 310.

(35) Hayden, B. E. In *Vibrational Spectroscopy of Molecules at Surfaces*; Yates, J. T., Madey, T. E., Eds.; Plenum: New York, 1987; Chapter 7.

(36) Ehlers, D. H.; Esser, A. P.; Spitzer, A.; Lüth, H. *Surf. Sci.* **1987**, *191*, 466.

(37) Persson, B. N. J., Ryberg, R. *Phys. Rev. B* **1981**, *24*, 6954.

(38) Luo, J. S.; Tobin, R. G.; Lambert, D. K. *Chem. Phys. Lett.* **1993**, *204*, 445.

(39) For overviews, see: (a) Hollins, P.; Pritchard, J. *Prog. Surf. Sci.* **1985**, *19*, 275. (b) Ueba, H. *Prog. Surf. Sci.* **1986**, *22*, 181. (c) Ryberg, R. *Adv. Chem. Phys.* **1989**, *76*, 1.

(40) Strictly speaking, α_e for water, as for other solvents, is anticipated to be dependent on molecular orientation. However, the degree of polarizability anisotropy for water is apparently small,[41] so that $\alpha_e \sim 1.5$ $Å^3$ regardless of the precise orientation of the solvent molecules surrounding the infrared-active chemisorbate. In addition, the refractive index (and therefore the polarizability) of liquid water is not altered substantially between visible optical and mid-infrared frequencies,[41] so that the applicability of the simple "electronic screening" model should not be affected by the presence of intramolecular motions occurring at higher wavenumbers than those corresponding to C−O chemisorbate vibrations.

(41) Hasted, J. B. In *Water—A Comprehensive Treatise*; Franks, F., Ed.; Plenum: New York, 1972; Vol. 1, Chapter. 7.

(42) Xu, Z.; Sherman, M. G.; Yates, J. T.; Antoniewicz, P. R. *Surf. Sci.* **1992**, *276*, 249.

(43) (a) Leibsle, F. M.; Sorbello, R. S.; Greenler, R. G. *Surf. Sci.* **1987**, *179*, 101. (b) Brandt, R. K.; Sorbello, R. S.; Greenler, R. G. *Surf. Sci.* **1992**, *271*, 605.

(44) Comrie, C. M.; Weinberg, W. H. *J. Chem. Phys.* **1976**, *64*, 250.

(45) It should be noted that the calculated $\Delta\nu_{1/2}$ values included in Figure 6 employ only a *single* isolated CO oscillator frequency (the "singleton" ν_{CO} value, 2000 cm^{-1}, used here), so that possible additional stochastic band-broadening effects arising from a statistical distribution of adsorbate binding sites are not included in these calculations. [While this additional band-broadening component was found to affect the bandwidth for multiply coordinated CO,[10b] it should be markedly less important for atop (or near-atop) CO geometries, as encountered here. (See ref 26 for a detailed discussion of this point).]

(46) (a) Persson, B. N. J. *J. Electron. Spectrosc. Relat. Phenom.* **1990**, *54/55*, 81. (b) Persson, B. N. J.; Hoffmann, F. M. *J. Electron. Spectrosc. Relat. Phenom.* **1987**, *45*, 215.

(47) For example: Bailey, R. T. In *Molecular-Spectroscopy-A Specialist Periodical Report*; Chemical Society: London, 1974; Vol. 2, Chapter 3.
(48) Corrigan, D. S.; Gao, P.; Leung, L.-W. H.; Weaver, M. J. *Langmuir* **1986**, *2*, 744.
(49) (a) Zou, S.; Weaver, M. J. *J. Phys. Chem*. **1996**, *100*, 4237. (b) Zou, S.; Gómez, R.; Weaver, M. J. *Langmuir*, **1997**, *13*, 6713.
(50) Christensen, P. A.; Hamnett, A. In *Comprehensive Chemical Kinetics*; Compton, R. G., Hamnett, A., Eds.; Elsevier: Amsterdam, 1989; Vol. 29, p 46.
(51) See, for example, Figure 3 of ref 35.
(52) This value was deduced from the bottom spectrum in Figure 2 of ref 18 (see erratum), after conversion to a $\log_{10}$ absorbance scale (see text).